

A pseudo-viscoelastic approach for transient polymeric flow exiting a channel

R. E. Khayat^{*,†} and N. Ashrafi

*Department of Mechanical and Materials Engineering, University of Western Ontario,
London, Ontario, Canada, N6A 5B9*

SUMMARY

The influence of elasticity of a fluid exiting a channel is examined on transient coating downstream. A hybrid spectral/boundary element approach is proposed to solve the problem. The flow inside the channel is assumed to be fully developed. A viscoelastic instability of one-dimensional plane Couette flow is first determined for a large class of Oldroyd fluids with added viscosity, which typically represent polymer solutions composed of a Newtonian solvent and a polymeric solute. The Johnson–Segalman equation is used as the constitutive model. The velocity profile inside the channel is taken as the exit profile for the emerging free-surface flow. The flow is assumed to be Newtonian as it emerges from the channel. An estimate of the magnitude of the rate-of-strain tensor components in the free-surface region reveals that they are generally smaller than the shear rate inside the channel. The evolution of the flow front is simulated using the boundary element method. For the channel flow, the problem is reduced to a nonlinear dynamical system using the Galerkin projection method. Stability analysis indicates that the channel velocity may be linear or non-linear depending on the range of the Weissenberg number. The evolution of the coating flow at the exit is examined for steady as well as transient (monotonic and oscillatory) channel flow. It is found that adverse flow can exist as a result of fluid elasticity, which can hinder the process of blade coating. Copyright © 2003 John Wiley & Sons, Ltd.

KEY WORDS: viscoelastic; coating flow; Johnson–Segalman; BEM

1. INTRODUCTION

Although steady coating flow has been extensively investigated, little effort has been devoted to transient behaviour. This is of course understandable since it is the long-term flow, after transient effects die out, which is of practical interest. However, when difficulties are encountered in a given coating process, the solution to the problems may lie in the initial stages of the process, long before the process reaches the steady state. It is thus important to exam-

*Correspondence to: R. E. Khayat, Department of Mechanical and Materials Engineering, University of Western Ontario, London, Ontario N6A 5B9, Canada.

†E-mail: rkhayat@eng.uwo.ca

Contract/grant sponsor: National Science and Engineering Research Council of Canada

ine the initial transients, which may allow early control of possible problems. There is also the issue regarding the time it takes for a coating process to reach steady state. This issue is particularly important for polymeric fluids, which exhibit different relaxation times, and, therefore, different transient response. Finally, the coating process can be inherently transient, and, consequently, may never settle into steady behaviour as a result of geometrical variations or constant changes in processing conditions. This work examines transient effects by focusing on the early stages of the blade coating process.

The coating process consists of applying a thin layer of fluid to a solid substrate. This process can be of practical relevance, for instance, to the electronics industry (where the eventual purpose of the layer is typically to store information) and to the paint industry (where the purpose is typically to form a protective layer). Most of the theoretical work so far concerning coating flows has concentrated on Newtonian fluids [1] and, to a much lesser extent, on non-Newtonian fluids, including viscoelastic and generalized Newtonian flows, touching processes in blade and roll coating (see Reference [2] and the references therein).

In this study, the modelling and simulation of the early stages of blade coating are examined in two dimensions. The fluid is initially confined between two plates, one of which is set in motion to induce the flow. The problem thus consists of obtaining the flow and stress fields inside a moving domain, as the fluid emerges from the channel. The study emphasizes the influence of exit flow, which is the fully developed flow inside the channel, on the emerging fluid. In the present problem, the lubrication assumption cannot be used since most of the interest lies in the vicinity of the flow front. In this region, the lubrication assumption cannot capture the details typical of free surface flow (fountain flow). In the present study, the flow at the front is captured accurately since the fluid is assumed to be thick everywhere in the domain (away and near the front).

The velocity profile inside the channel constitutes the major non-homogeneous boundary condition for the moving domain problem. In this study, the plane Couette flow (PCF) is assumed to be fully developed and obeys the Johnson–Segalman (JS) constitutive model [3, 4]. The presence of elasticity is expected to drastically alter the stability and bifurcation picture in PCF, and yet no study has so far predicted the nonlinear bifurcation from the base flow. Similarly to the case of Taylor–Couette flow, there is experimental evidence that the base flow in a channel may lose its stability as a result of fluid elasticity inside the tube [5]. This type of instability is known as constitutive instability in the literature, as opposed to slip-induced instability. The emergence of surface instability at the exit of an extrusion die (sharkskin and melt fracture) suggests the possibility of a link with a hydrodynamic instability inside the channel, away and upstream from the exit [6]. More recent studies based on more generalized constitutive models of the *Oldroyd* class showed that the base flow in a channel can become unstable to small perturbations for some range of Weissenberg numbers [7–9]. These generalized constitutive models display a non-monotonic shear–stress/shear–rate curve. The range of instability coincides with the negative slope of the stress curve. The choice of a viscoelastic constitutive model for the present problem is crucial. The more interesting response of transient blade coating is expected to emerge when nonlinear channel flow is considered. The JS equation is ideal in this case as it leads to multiple nonlinear profiles in the critical range of Weissenberg numbers [10, 11]. These profiles, along with the stability and bifurcation diagrams, have been extensively investigated recently [11]. The method of solution was based on the Galerkin projection method and low-order dynamical systems. These techniques have been explored by Khayat [12] for various non-linear and non-Newtonian problems in

hydrodynamic stability. In this paper, only a summary of methodology and results relevant to fully developed PCF are reported, leaving the details to Reference [11].

Once the channel velocity profile is imposed at the exit, the flow field of the emerging fluid can be determined. This is a problem of the moving boundary type, and its solution remains challenging [13, 14], particularly when nonlinear viscoelastic effects are included, in addition to geometrical nonlinearities. Several numerical techniques have been developed for the solution of moving boundary/initial value problems. The boundary-element method (BEM) is much easier to use than domain methods, especially for moving-domain problems. The present paper is part of a series of studies on the applicability of the BEM to problems of the moving-boundary type. The reader is referred to Khayat *et al.* [15] for a review.

2. PROBLEM FORMULATION AND SOLUTION FOR CHANNEL FLOW

In this section, only the flow inside the channel is examined (Figure 1). A summary of problem formulation is given for the channel flow of a Johnson–Segalman (JS) fluid. Details of formulation and solution procedure as well as additional results are given elsewhere [11]. Only one-dimensional flow is considered. The resulting equations are solved using the Galerkin projection.

Consider the PCF of an incompressible viscoelastic fluid of density ρ , relaxation time λ , surface tension γ , and viscosity η . In this study, only fluids that can be reasonably represented by a single relaxation time and constant viscosity are considered. The fluid considered here is a polymer solution composed of a Newtonian solvent and a polymer solute of viscosities η_s and η_p , respectively. Therefore $\eta = \eta_s + \eta_p$. The channel flow is induced by the translation of the lower plate, which move at velocity U , with the upper plate remaining stationary. The velocity, time, space co-ordinates, and stress/pressure are non-dimensionalized by d/λ , λ , d , and η_p/λ , respectively, where d is the gap between the two channel plates. There are three important similarity groups in the problem, namely, the Reynolds number, Re , the Weissenberg number, We , the solvent-to-solute viscosity ratio, ε , and the capillary number, which are given, respectively, by

$$Re = \frac{d^2 \rho}{\eta_p \lambda}, \quad We = \frac{U \lambda}{d}, \quad \varepsilon = \frac{\eta_s}{\eta_p}, \quad Ca = \frac{\lambda \gamma}{\eta_p d} \quad (1)$$

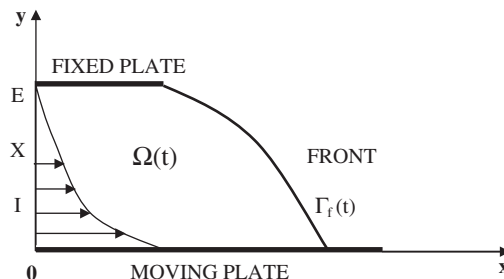


Figure 1. Schematic illustration of the domain of computation and notation for the boundary-integral method.

In this work, the stress is taken to be the combination of a Newtonian and a polymeric contribution. The constitutive equation adopted in this study is the JS model, which belongs to the Oldroyd class of incompressible viscoelastic fluids [11].

If the x -axis is taken to lie half-way between the two plates, and y is the co-ordinate in the transverse direction, then the total shear stress corresponding to the base (Couette) flow is given by

$$T_{xy}^b = \varepsilon We + \frac{We}{1 + \zeta(2 - \zeta)We^2} \quad (2)$$

Here $\zeta \in [0, 2]$ and is a dimensionless material (slip) parameter. Note that We is a measure of the shear rate since the velocity, $u(y, t)$, at the two plates is given by $u(y=0, t) = We$ and $u(y=1, t) = 0$. Equation (2) is perhaps the most revealing result of the JS model. It reflects the possibility of a non-monotonic behaviour for the stress/shear-rate relation. Indeed, the stress generally exhibits two extrema (a maximum and a minimum) when plotted against We , which tend to merge as ε increases (see Reference [11]). This situation is reminiscent of the load/deformation behaviour in elasticity. In the case of non-linear inflation of a Mooney–Rivlin (hyperelastic) membrane, for instance, the pressure also exhibits a similar behaviour as function of the stretch ratio for various Mooney constants [16]. The curve for $\varepsilon=0$ is comparable to that of a Neo-Hookean solid, while the curve for a Newtonian fluid ($\varepsilon=1$) is comparable to the curve of a Hookean solid (see Figure 2 in Reference [16]).

For one-dimensional disturbance along the channel (x -axis), the departure (from base flow) is reduced to the axial velocity, $u(y, t)$, normal stress difference, $N(y, t)$, and shear stress, $S(y, t)$. In this case, the relevant equations for the problem reduce to

$$Re u_t = \varepsilon u_{yy} + S_y, \quad (3a)$$

$$N_t = -N + 2(WeS + Su_y + S^b u_y) \quad (3b)$$

$$S_t = -S + u_y + a(WeN + Nu_y + N^b u_y) \quad (3c)$$

where $a = \zeta((\zeta/2) - 1)$, $S^b = We/(1 + \zeta(2 - \zeta)We^2)$ is the non-Newtonian contribution of the shear stress of the base flow, and $N^b = 2We^2/(1 + \zeta(2 - \zeta)We^2)$ is the corresponding first normal stress difference. A subscript in Equation (3) denotes partial differentiation. It is important to observe that if there is no external (mean) pressure imposed inside the channel, the departure of pressure is also zero. The flow departure is represented by series of Chandrasekhar functions, which satisfy the homogeneous (no-slip) boundary conditions [11].

The solution of Equations (3) is carried out using the Galerkin projection method. The variables $u(y, t)$, $N(y, t)$ and $S(y, t)$ are represented in series of Chandrasekhar functions that satisfy the homogeneous (no-slip) boundary conditions. A suitable level of truncation is imposed, which leads to the final nonlinear dynamical system. A judicious selection process is applied for the choice of the various modes in order to ensure the physical and mathematical coherence of the final model. The first step in the Galerkin projection method consists then of multiplying each of Equations (3) by the appropriate mode and is integrated over the mapped interval $[-\frac{1}{2}, \frac{1}{2}]$. One thus obtains a set of nonlinear and coupled ordinary differential equations that govern the time-dependent expansion coefficients. The solution of the resulting nonlinear dynamical system is obtained after a suitable truncation level is introduced, i.e.

after a suitable number of modes, M , is assumed. Assessment of convergence was previously conducted [11], and it was found that convergence is reached for $M > 6$. Comparison against the finite-element results of Georgiou and Vlassopoulos [10] showed that the 'exact' velocity profiles, including discontinuities, can be captured by a small number of modes. In addition, the overall stability and bifurcation picture is not significantly influenced by the number of modes adopted, and that expansion of the flow field with $M = 2$ lead to qualitatively accurate results. Thus, most of the profiles reported below are based on two-mode expansions.

Linear stability analysis indicates the existence of two critical Weissenberg numbers, We_{c1} and We_{c2} , where an exchange of stability occurs between the base (linear) flow and a nonlinear Couette flow. The range $We < We_{c1}$ will be referred to as the pre-critical range, $We_{c1} < We < We_{c2}$ as the critical range, and $We > We_{c2}$ as the post-critical range. For a typical fluid, $\zeta = 0.2$, $\varepsilon = 0.04$, the base flow loses its stability to nonlinear flow at $We_{c1} = 1.89$ and recovers linear behaviour at $We_{c2} = 7.78$. The base flow is thus stable for both the pre-critical and post-critical ranges. While the (steady) flow in the pre- and post-critical ranges is unique, there is a multitude of solution branches in the critical region [11].

In practice, it is well known that in real systems, physical instabilities are observed when the flow rate and/or the level of elasticity are high. Both the flow rate and fluid elasticity are the determining factors behind the destabilization of the base flow. Recall that the flow rate is controlled by We , and the level of elasticity by both We and ζ . Finally, the stability picture near We_{c1} and We_{c2} was established numerically since linear stability analysis cannot be applied in the vicinity of the critical points, which are non-hyperbolic fixed points. A multiple-scale analysis was also carried out to confirm the numerical results [11].

3. PROBLEM FORMULATION FOR FREE-SURFACE FLOW

In this section, the governing equations and boundary conditions are reviewed together with some of the assumptions taken for the blade-coating flow. For simplicity, the fluid is assumed to be viscous incompressible and Newtonian as it emerges from the channel. Only low-Reynolds-number flow, typically characterized by small velocities, small length scales and/or high viscosity, will be considered. In this limit, the inertia terms in the momentum equation are negligible, so the flow is in a state of creeping motion.

3.1. Problem statement and governing equations

With the fully developed channel flow established from the previous section, the evolution of the free surface flow is now sought as the fluid emerges from the channel. The problem at the exit is a difficult one given the transient nature of the flow and the presence of a free surface. Although conventional methods, such as the finite-difference and finite-element methods, are well adapted to handle complex non-linear flow configurations, these methods are inadequate for moving boundary problems, given their requirement for adaptive meshing and remeshing. From this standpoint, the BEM is much more convenient since only the boundary needs to be discretized, but the BEM is essentially inadequate to handle nonlinear flow. This is a major problem that still plagues the BEM despite recent developments in the so-called 'non-linear' techniques [17] order to apply the BEM, it is assumed that the flow at the exit behaves like a Newtonian flow. This is not an unreasonable assumption given the relatively low shear and

elongation rates that the fluid experiences after it leaves the channel (see Section 6). Inertia is neglected as well, so the flow is in a state of creeping motion.

At any instant, t , the fluid is assumed to occupy a 2D region, $\Omega(t)$, which is bounded by $\Gamma(t)$. It is convenient to take $\Omega(t)$ as the inner domain, excluding $\Gamma(t)$. The fluid is taken to be neutrally buoyant so the effects of gravity and any external body forces are negligible. The conservation of mass and linear momentum equations are (in dimensionless form) given by

$$\nabla \cdot \mathbf{u}(\mathbf{x}, t) = 0, \quad \nabla \cdot \boldsymbol{\sigma}(\mathbf{x}, t) = \mathbf{0}, \quad \mathbf{x} \in \Omega(t) \cup \Gamma(t) \quad (4)$$

where $\mathbf{x}(x, y)$ the position vector in the (x, y) plane, $\mathbf{u}(\mathbf{x}, t)$ the velocity vector, and $\boldsymbol{\sigma}(\mathbf{x}, t)$ is the total stress tensor given in terms of the hydrostatic pressure $p(\mathbf{x}, t)$ and the rate-of-strain tensor. Thus, although the fluid is Newtonian, it is still assumed to be composed of a solvent and a solute of viscosities η_s and η_p , respectively, and a combined viscosity $\eta = \eta_s + \eta_p$. In this case, the dimensionless stress is given by

$$\boldsymbol{\sigma}(\mathbf{x}, t) = -p(\mathbf{x}, t)\mathbf{I} + (\varepsilon + 1)[\nabla\mathbf{u}(\mathbf{x}, t) + \nabla\mathbf{u}^t(\mathbf{x}, t)], \quad \mathbf{x} \in \Omega(t) \cup \Gamma(t) \quad (5)$$

where \mathbf{I} is the unit tensor. It is important to note that the acceleration term $\partial\mathbf{u}/\partial t$ in the momentum conservation equation has been neglected, so that for a Newtonian fluid, the formulation in question is not strictly unsteady, but quasi-steady. This quasi-steady state assumption is valid whenever $L^2/v \ll T$, where L and T are typical characteristic length and time of the flow, and $v = \eta/\rho$ is the kinematic viscosity. In the present case, $T \sim L/U$, U being a typical value of the driving velocity. Thus, for the quasi-steady state assumption to apply, one must have $UL/v \ll 1$. This is indeed typically the case for fluids of interest to coating problems. Physically, the quasi-steady state approximation means that a Newtonian fluid immediately adjusts to changes in the movement of the boundary or boundary conditions.

3.2. Boundary and initial conditions

The boundary $\Gamma(t)$ is composed of part of the channel, $\Gamma_c(t)$, and the free surface, $\Gamma_f(t)$. Note that $\Gamma_c(t)$ changes with time as the fluid emerges out of the channel and spreads on the lower plate. Thus, $\Gamma(t) = \Gamma_c(t) \cup \Gamma_f(t)$. While the boundary conditions on $\Gamma_c(t)$ are straightforward to implement, those on $\Gamma_f(t)$ must be examined more closely. The fluid is assumed to adhere to the channel walls, so that stick boundary conditions apply. More generally, the velocity is assumed to be fully prescribed on $\Gamma_c(t)$. The fluid is assumed to obey plane Couette flow at the exit of the channel. In addition, the stick and no-penetration conditions hold at the walls of the channel. These conditions may be written compactly in the form

$$\mathbf{u}(\mathbf{x}, t) = \mathbf{u}_c(\mathbf{x}), \quad \mathbf{x} \in \Gamma_c(t) \quad (6)$$

Thus, the flow field is determined through the solution of Equations (4) and (5), which is obtained subject to condition (6), and the dynamic and kinematic conditions on $\Gamma_f(t)$. The proper choice and implementation of a kinematic condition is generally not obvious [1].

Regarding the kinematic condition on the free surface, the front is assumed to deform with the fluid velocity, such that

$$\frac{d\mathbf{x}}{dt} = \mathbf{u}(\mathbf{x}, t), \quad \mathbf{x} \in \Gamma_f(t) \quad (7)$$

The dynamic condition on the free surface are based on the continuity of the tangential stress (no traction) and discontinuity of normal stress caused by the surface tension, and thus

$$\mathbf{t}(\mathbf{x}, t) = \text{Ca}^{-1} \mathbf{n}(\mathbf{x}, t) \nabla \cdot \mathbf{n}(\mathbf{x}, t), \quad \mathbf{x} \in \Gamma_f(t) \quad (8)$$

where $\mathbf{t}(\mathbf{x}, t) = \boldsymbol{\sigma}(\mathbf{x}, t) \cdot \mathbf{n}(\mathbf{x}, t)$ is the traction, and \mathbf{n} is the normal unit vector at the front. Note that boundary condition (8) is derived under conditions of equilibrium and uniform surface tension, and its validity under dynamic conditions is simply assumed. The condition also assumes implicitly that the flow activity of the fluid outside the free surface (air) is negligible with the (atmospheric) pressure taken as zero.

Finally, an initial condition is needed. In this study, the fluid is assumed to be at rest initially, so that the following condition holds:

$$\mathbf{u}(\mathbf{x}, t = 0) \equiv \mathbf{0}, \quad \mathbf{x} \in \Omega(t = 0) \cup \Gamma(t = 0) \quad (9)$$

System (4)–(5), subject to conditions (6)–(9), constitute a well-posed problem.

3.3. Boundary integral equation

The general time-dependent-integral equation for a moving domain is given by (Power and Wrobel, 1995):

$$\begin{aligned} & \int_{\Gamma(t)} \mathbf{t}(\mathbf{y}, t) \cdot \mathbf{J}(\mathbf{x}|\mathbf{y}) \, d\Gamma_{\mathbf{y}} \\ & - \int_{\Gamma(t)} \mathbf{n}(\mathbf{y}, t) \cdot \mathbf{u}(\mathbf{y}, t) \cdot \mathbf{K}(\mathbf{x}|\mathbf{y}) \, d\Gamma_{\mathbf{y}} = c(\mathbf{x}, t) \cdot \mathbf{u}(\mathbf{x}, t), \quad \mathbf{x} \in \Omega(t) \cup \Gamma(t) \end{aligned} \quad (10)$$

where \mathbf{J} and \mathbf{K} are the usual symmetric and anti-symmetric tensors with respect to relative position $\mathbf{r} = \mathbf{x} - \mathbf{y}$ of two points at \mathbf{x} and \mathbf{y} , and are given as (Power and Wrobel 1995):

$$\mathbf{J}(\mathbf{x}|\mathbf{y}) = \frac{1}{4\pi} \left(\mathbf{I} \log r - \frac{\mathbf{r}\mathbf{r}}{r^2} \right), \quad \mathbf{K}(\mathbf{x}|\mathbf{y}) = -\frac{1}{\pi} \frac{\mathbf{r}\mathbf{r}\mathbf{r}}{r^4} \quad (11)$$

where $r = |\mathbf{r}|$. The function $c(\mathbf{x}, t)$, for $\mathbf{x} \in \Gamma(t)$, depends on the geometrical form of the boundary; its value arises from the jump in the value of the velocity integrals as the boundary is crossed. When the boundary is Lyapunov smooth, which requires that a local tangent to the moving boundary exists everywhere, the function $c(\mathbf{x}, t) = 1/2$. This is the case if constant boundary elements are used. Thus, the assumption of boundary smoothness is generally not valid in the vicinity of sharp corners, cusps or edges. In general, since $c(\mathbf{x}, t)$ depends solely on geometry, it may be evaluated assuming that a uniform velocity field such as $\mathbf{u}(\mathbf{x}, t) = \mathbf{u}\mathbf{e}$ is applied over the boundary, \mathbf{e} being the direction of the velocity and \mathbf{u} is its magnitude. Under these conditions, all derivatives (including tractions and stresses) must vanish. Hence, at any time t , Equation (11) reduces to

$$c(\mathbf{x}, t) = \int_{\Gamma(t)} \mathbf{n}(\mathbf{y}, t) \cdot [\mathbf{e} \cdot \mathbf{K}(\mathbf{x}|\mathbf{y}) \cdot \mathbf{e}] \, d\Gamma_{\mathbf{y}}, \quad \mathbf{x} \in \Gamma(t) \quad (12)$$

Thus, at any time t , the form of the boundary $\Gamma(t)$ is determined, and the function $c(\mathbf{x}, t)$ is evaluated using Equation (12). The boundary integral equation (10) governs the flow variables

at the boundary. It relates the velocity to the traction on $\Gamma(t)$. The traction is determined wherever the velocity is imposed and vice versa. Hence, at the free surface, where the traction is specified, the velocity will be calculated. For the rest of the boundary, at the moving wall and channel exit, the velocity is specified and the traction is determined.

4. SOLUTION PROCEDURE

In this section, a time-marching scheme is proposed to discretize Equation (7). Once the flow field is determined at a given time step from Equation (10), the location of the free surface can be determined by solving Equation (7). As the boundary elements are distorted, the mesh is refined through element subdivision. Consider the application of the integral equation (10) for a point on the boundary, that is, for $\mathbf{x} \in \Gamma(t) = \Gamma_c(t) \cup \Gamma_f(t)$. The flow field at any interior point $\mathbf{x} \in \Omega(t)$ can be obtained once the flow variables at the boundary are known. Since the velocity is fully prescribed on $\Gamma_c(t)$, only the traction will be determined there. The traction is imposed on the moving boundary, $\Gamma_f(t)$, where the value of the velocity will be found. More explicitly, Equation (10) may be rewritten as

$$\begin{aligned} & \int_{\Gamma_c(t)} \mathbf{t}(\mathbf{y}, t) \cdot \mathbf{J}(\mathbf{x}|\mathbf{y}) \, d\Gamma_y - \int_{\Gamma_f(t)} \mathbf{u}(\mathbf{y}, t) \cdot [\mathbf{n}(\mathbf{y}, t) \cdot \mathbf{K}(\mathbf{x}|\mathbf{y})] \, d\Gamma_y \\ & + \text{Ca}^{-1} \int_{\Gamma_f(t)} [\mathbf{n}(\mathbf{y}, t) \nabla \cdot \mathbf{n}(\mathbf{y}, t)] \cdot \mathbf{J}(\mathbf{x}|\mathbf{y}) \, d\Gamma_y \\ & - \int_{\Gamma_c(t)} \mathbf{u}_c(\mathbf{y}) \cdot [\mathbf{n}(\mathbf{y}) \cdot \mathbf{K}(\mathbf{x}|\mathbf{y})] \, d\Gamma_y = \begin{cases} c(\mathbf{x}, t) \mathbf{u}_c(\mathbf{x}), & \mathbf{x} \in \Gamma_c(t) \\ c(\mathbf{x}, t) \mathbf{u}(\mathbf{x}, t), & \mathbf{x} \in \Gamma_f(t) \end{cases} \end{aligned} \quad (13)$$

where conditions (6) and (9) are used. The unknowns in Equation (13) are thus $\mathbf{t}(\mathbf{x}, t)$ for $\mathbf{x} \in \Gamma_c(t)$ and $\mathbf{u}(\mathbf{x}, t)$ for $\mathbf{x} \in \Gamma_f(t)$, so that the values of the third and fourth integrals are known.

The evolution of the free surface is determined by solving Equation (7). The time derivative in the equation is approximated by an explicit Eulerian finite-difference scheme. Let Δt be the time increment, so that at time $t = k \Delta t$, the new position, \mathbf{x}_k , of a point on the free surface is given by

$$\mathbf{x}_k = \mathbf{x}_{k-1} + \mathbf{u}_{k-1}(\mathbf{x}_{k-1}) \Delta t + O(\Delta t) \quad \mathbf{x} \in \Gamma_f(t) \quad (14)$$

where $\mathbf{u}_{k-1}(\mathbf{x}_{k-1}) = \mathbf{u}[\mathbf{x} = \mathbf{x}_{k-1}, t = (k-1)\Delta t]$ is the velocity of the point at the previous time step. The integral equation (14) relates the velocity and traction at the current time. Once the flow field is determined at each time step, t , the position of the moving boundary is updated. The evolution of $\Gamma_f(t)$ is dictated by Equation (14). The updated position of the nodes that belong to the free surface is thus determined once the velocity at the front is obtained from the solution of Equation (13).

The integrals in Equation (13) are discretized into a finite sum of contributing terms over the boundaries. In this work, the boundary elements are assumed to be geometrically linear so that the velocity and traction are constant over each element. This makes the proposed adaptive remeshing method and estimation of curvature less difficult to implement since no interpolation

of the flow variables is needed at each time step. The use of higher-order elements is possible, but may not be crucial given the mesh refinement and remeshing capabilities involved in the current procedure. The traction is constant over flat linear element, and is multiply valued at a corner node if higher-order elements are used. In two dimensions, the traction is assumed to be double valued at every node of a curved boundary. Another advantage of the constant boundary element is that the value of $c(\mathbf{x}, t)$ is always and everywhere equal to $\frac{1}{2}$. In addition, the normal vector to each element is determined exactly.

5. NUMERICAL RESULTS

In this section the transient behaviour of the flow is explored for different exit conditions as the fluid emerges out of the channel. These conditions are based on the behaviour of fully developed JS fluid (upstream) inside the channel. Both pre-critical and critical profiles will be considered for the Couette flow as We is varied. The flow at the exit of the channel may be steady or unsteady, but in practice, it is the latter that is encountered. This is the case, for instance, when the lower plate is suddenly incepted from rest. The influence of both steady and unsteady input profiles will be considered on the developing free surface flow. For simplicity, surface tension effect will be assumed negligible.

5.1. Response of a steady exit flow

Consider the response of the coating flow to steady Couette at the exit of the channel. The objective of this section is to examine the influence of fluid elasticity on the emergence of free surface flow in the early stages of coating. For simplicity, the profile inside the channel, and at the exit ($x=0$), is assumed to be fully developed, although the emerging flow corresponds to the sudden inception of the lower plate. Thus, the flow inside the channel is assumed to respond instantly to the inception. The domain of calculation is initially the unit square $(x, y) \in [0, 1] \times [0, 1]$. Only the Weissenberg number is varied and the rest of the parameters are fixed to $Re = 1$, $\zeta = 0.2$ and $\varepsilon = 0.04$. In this case, the two critical Weissenberg numbers are $We_{c1} = 1.89$ and $We_{c2} = 7.78$, so that the pre-critical, critical and post-critical ranges correspond, respectively, to $We < 1.89$, $1.89 < We < 7.78$, and $We > 7.78$.

The results corresponding to the pre-critical and critical ranges are displayed in Figure 2 for $We \in [1, 7]$. Note that the response in the post-critical range is the same as that in the pre-critical range since the Couette profile is the same in the two ranges. In all cases, the Couette profile is included for reference (dashed curve) in addition to the free surface profiles at the early time stages of flow. Note that the velocity profile is normalized for comparison with the case $We = 1$. The response in the pre-critical range is typically illustrated by the $We = 1$ flow. In this case, the Couette flow is linear, similarly to Newtonian flow. Right at the inception, and as expected, the free surface is initially linear with respect to y , similarly to the Couette profile. As the fluid emerges out of the channel, the shape of the melt front begins to deviate from the linear profile and assumes a curved shape. The bulk of the fluid trails further the fluid in the immediate vicinity of the moving lower plate. After some time, the profile concavity changes, and the front tends to bulge out. Numerical instabilities of the saw-tooth type are observed, which are usually controlled by applying the smoothing technique.

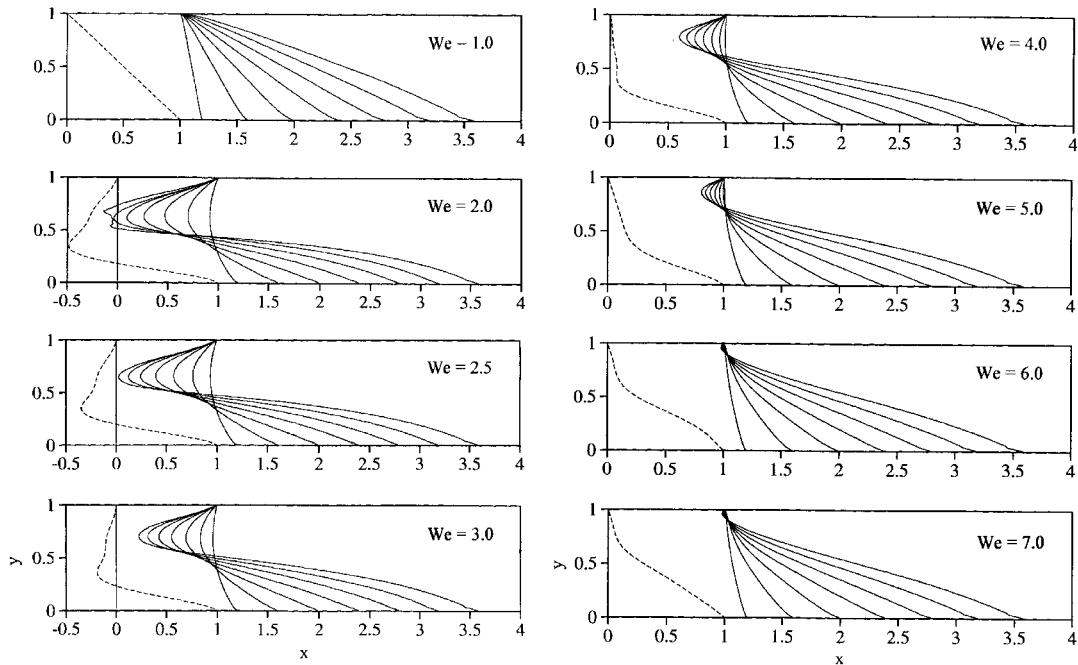


Figure 2. Response to steady Couette flow at the channel exit (dashed line). Evolution of the free surface for various values of the Weissenberg number ($Re = 1$, $\zeta = 0.2$ and $\varepsilon = 0.04$) in the pre-critical range ($We < 1.89$), and critical range ($1.89 < We < 7.78$).

In the present case, however, the instability remained localized (close to the lower plate), and did not necessitate smoothing.

In the critical range, the Couette profile becomes non-linear. In this case, there is a multiplicity of solution branches. Each steady velocity profile depends on the initial conditions used to reach it. This statement may at first appear meaningless since a steady-state solution does not generally depend on initial conditions. However, when more than one steady-state solution exist, each solution may correspond to a set of initial conditions. In the present problem, the initial conditions correspond to the initial perturbation from the base flow. In this study, the Couette profiles are taken to correspond to a flow with an initial sudden inception. The influence of fluid elasticity in the critical range is depicted in Figure 2 for $We = 2, 2.5, 3, 4, 5, 6$ and 7 . All profiles at the channel exit are non-linear as indicated by the dashed curves in the figure. As We exceeds $We_{c1} = 1.89$, a dramatically different Couette profile is found as indicated for $We = 2$. The response of the coating flow is initially almost linear, but it begins to exhibit an adverse behaviour near the stationary plate. In fact, a significant portion of the fluid actually moves in the opposite direction of the main stream. The flow exhibits a vortex structure similar to lid-driven cavity flow.

As elastic effects increase, the adverse flow decreases in intensity. The flow at the channel exit begins to show a reduction in backward motion. The coating flow adjusts to the exit profile, and more flow begins to move forward with the lower plate (see the flows corresponding to $We = 2.5$ and 3). The flow for this range of Weissenberg numbers clearly indicates

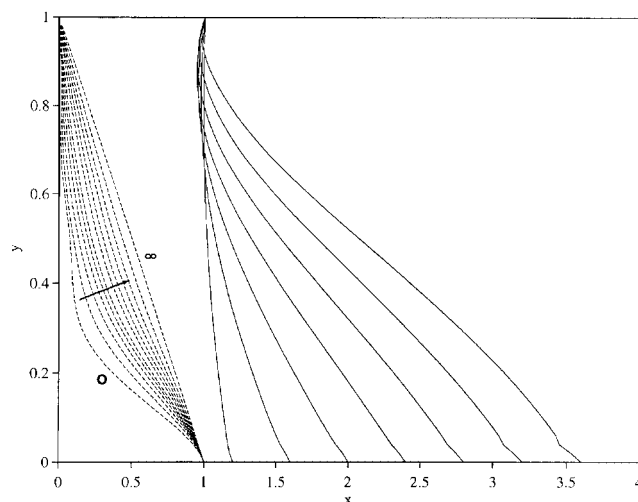


Figure 3. Response to transient Couette flow at the channel exit. The figure shows the development of the exit flow (dashed lines) from sudden inception. Evolution of the free surface (solid lines) for $We = 1$, $Re = 0.1$, $\zeta = 0.2$ and $\varepsilon = 0.04$.

a difficulty in coating a plate right after the onset of instability. In practice, this difficulty may translate into the impossibility of coating a material once the flow has reached a critical Weissenberg number, for instance, as a result of plate acceleration. As We increases further, the adverse flow disappears completely in the channel flow as depicted for $We = 4, 6$ and 7 . However, the free surface flow still experiences backward motion, with the flow gradually resembling that corresponding to $We = 1$. Finally, after We exceeds the second critical Weissenberg number, $We_{c2} = 7.78$, the base flow becomes stable once again, and a linear exit profile is again observed just like the pre-critical case. The flow exhibited in Figure 2 bears a strong resemblance two-dimensional cavity flow. In that case, the back flow emerges as a result of the presence of lateral boundaries.

5.2. Transient response to the inlet flow

Consider now the influence of a developing channel flow on the emerging fluid. Unlike the previous section, the exit flow is assumed to evolve from rest under sudden inception. The influence of the Reynolds number in this case is important since the acceleration term in Equation (3a) is no longer zero. It is generally found that the evolution of channel flow toward the steady state is monotonic when Re is small, and it is oscillatory when Re is relatively large. Two cases will be considered next to illustrate the influence of Re on coating in the pre-critical and critical ranges of the Weissenberg number. The evolution of the flow inside and outside the channel is followed from rest, at time $t = 0$, when the flow is induced by sudden inception, until the time when the channel flow reaches the steady state.

Consider again the pre-critical case, $We = 1$ and $Re = 0.1$. In this case, the channel flow is expected to evolve monotonically to the linear Couette flow as depicted from Figure 3. The figure is not drawn to scale for clarity. The arrow indicates the direction of flow development

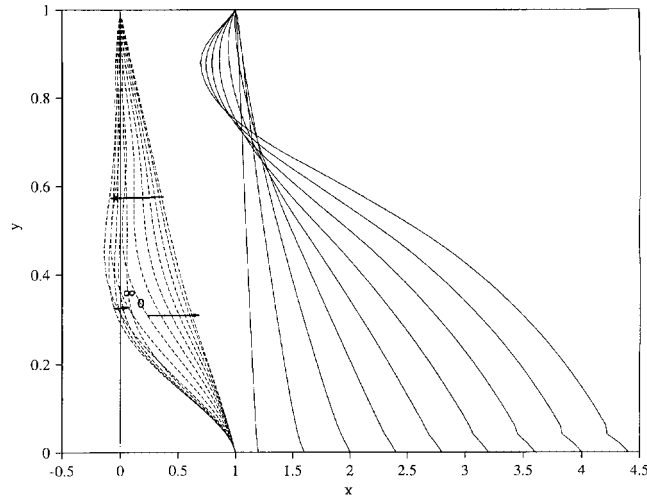


Figure 4. Response to transient Couette flow at the channel exit. The figure shows the development of the exit flow (dashed lines) from sudden inception. Evolution of the free surface (solid lines) for $We = 4$, $Re = 1$, $\zeta = 0.2$ and $\varepsilon = 0.04$.

inside the channel. The figure shows that the response of the coating flow differs from that in Figure 2 for the same Weissenberg number ($We = 1$). Unlike the response to steady (linear) Couette flow, in this case the front exhibits some initial back flow, but eventually changes concavity to become similar to the later stages in Figure 2. The bulk behaviour is, however, essentially the same in both cases.

In the critical range, oscillatory behaviour is easier to detect, as typically illustrated in Figure 4 for $We = 4$ and $Re = 1$. The arrows in the figure indicate the sense of time evolution of the channel flow. Initially, there is a sudden jump to (almost) linear Couette flow inside the channel. This is also confirmed from the first curve shown for the front. There is a significant adverse flow that develops with time. However, it may not be as strong as in the case $We = 4$ shown in Figure 2 for steady exit flow. Note that complete steady state is not fully restored inside the channel (although it is indicated by ∞ in Figure 4); much longer time is needed to reach the state shown in Figure 2. The oscillation in channel flow is inferred by the sense of the arrows. Finally, it is important to observe, from Figures 2 ($We = 4$) and 6, that transient channel flow appears to have minimal effect on the overall evolution of the coating process.

6. DISCUSSION

The major point that is being addressed in this discussion is the assumption adopted in the present formulation to consider the flow as Newtonian as it emerges from the channel. Several arguments can be used to justify this assumption, but the argument of scale, and that regarding the change in flow conditions at the channel exit are the main ones. It is made clear that the assumption can be limiting, and it is adopted here, like most common assumptions, for practical reasons. First, consider the change in flow conditions.

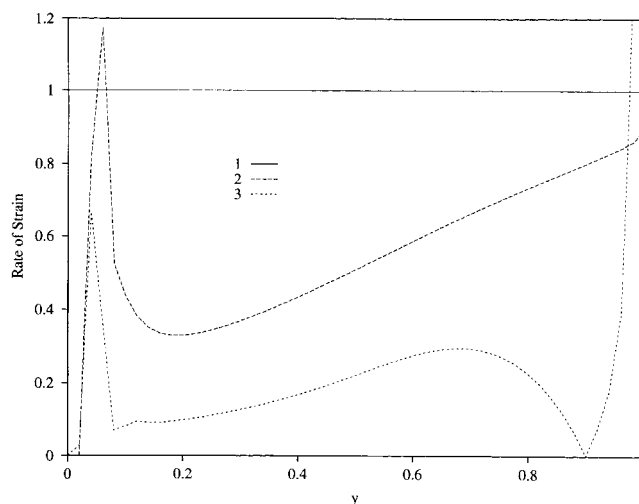


Figure 5. Relative magnitude of shear and normal strain rates at the final front for a flow in the pre-critical range ($We = 1$, $Re = 1$, $\zeta = 0.2$ and $\varepsilon = 0.04$). The figure shows (for reference) the shear rate at the channel exit (1), and at the front, the overall shear rate (2), the distribution of $|\partial v/\partial y|$ (3).

In many flow configurations, overall flow conditions may change with time or from one location to the other. The present blade-coating flow in Figure 1 is a striking reflection of the latter case. The problem of die flow is another illustration, but there is an important difference between the two flows as will be argued shortly. Viscoelastic effects become significant whenever shear and/or elongation flow is significant. As the fluid exits the channel, there is a dramatic drop in shear rate. In fact, the free surface flow, because of the adherence conditions at the moving plate, is expected to move almost like a rigid body. Given the absence of a driving pressure, or, more importantly, the lack of mechanism for elongation flow, normal stress effects are also not expected to be important. This is in sharp contrast with the die swell problem, which exhibits a sudden expansion of the flow induced by normal stresses. In blade coating, the absence of hydrostatic pressure causes normal stresses to reduce significantly in the free-surface flow region, especially at the free surface itself, since pressure must be balanced by normal stress for the traction to vanish (assuming negligible surface tension effect). It is the magnitude of $u_x \equiv \partial u/\partial x$, or $v_y \equiv \partial v/\partial y$, that is crucial here, since it is directly related to the magnitude of the (elastic) normal stress difference.

The assessment of the magnitude of the rate-of-strain tensor components, including that of the average shear rate, is assessed upon comparison against the magnitude of the shear rate at the channel exit. Three typical ranges of flow are considered for the assessment of magnitude of the rate of strain, namely the pre-critical range, the critical range and moderately critical range. The comparison is typified in Figures 5–7 for $We = 1$, 4 and 7, respectively. These three flows correspond exactly to those in Figure 2, with $Re = 1$, $\varepsilon = 0.04$ and $\zeta = 0.2$. The distribution, with position y , of the magnitude of the shear rate at the channel is included in the figures for reference. The average shear rate is estimated by monitoring the ratio of the difference in the horizontal velocities at the plate and at the free surface over the free surface height. The figures show, along the free surface, the distributions of the magnitude of the

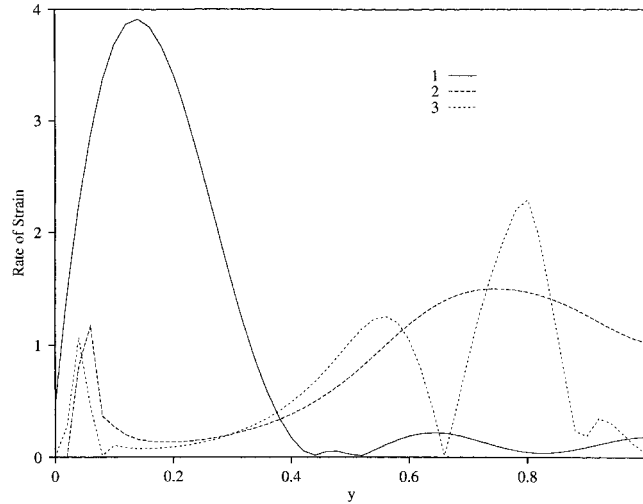


Figure 6. Relative magnitude of shear and normal strain rates at the final front for a flow in the highly critical range ($We = 4$, $Re = 1$, $\zeta = 0.2$ and $\varepsilon = 0.04$). The figure shows (for reference) the shear rate at the channel exit (1), and at the front, the overall shear rate (2), and the distribution of $|\partial v / \partial y|$ (3).

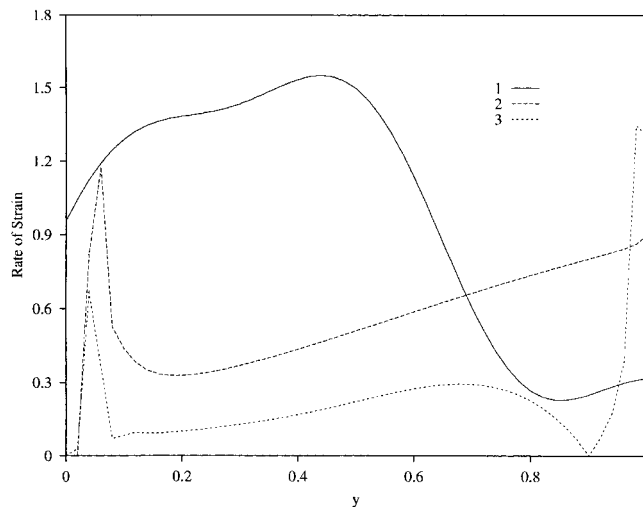


Figure 7. Relative magnitude of shear and normal strain rates at the final front for a flow in the moderately critical range ($We = 7$, $Re = 1$, $\zeta = 0.2$ and $\varepsilon = 0.04$). The figure shows (for reference) the shear rate at the channel exit (1), and at the front, the overall shear rate (2), and the distribution of $|\partial v / \partial y|$ (3).

average shear rate (2), as well as $|v_y|$ (3). For pre-critical flow ($We = 1$), the shear rate at the channel exit is constant and is equal to one as depicted from Figure 5. The figure shows that the average shear rate in the free surface flow region is roughly twice smaller than the exit shear rate, except perhaps near the channel exit and at the front tip where a singularity

develops. The quantity $|v_y|$ is even smaller, roughly one order of magnitude smaller than the shear rate at the exit. The comparisons for $We = 4$ (Figure 6) and $We = 7$ (Figure 7) lead to similar observations. Recall that for $We > 8$, one recovers the same flow configuration of the pre-critical range. In conclusion, the magnitude of the rate-of-strain components appears to be generally smaller than that of the shear rate at the channel exit. The normal components are one order of magnitude smaller. This comparison should be indicative of the relative insignificance of elastic effects in the free-surface flow region.

A scale argument can also be used to assess normal stress effects, by considering the value of the Weissenberg number, $We = U\lambda/d$. For a given fluid, with λ being fixed, the value of We is large whenever the typical velocity, U , of the fluid is large, or whenever the typical length, d , is small. In other words, the overall shear rate must be large for We or normal stress effects to be significant. As the fluid exits the channel, the characteristic velocity remains of the same order as inside the channel. The relaxation time does not change since the fluid in question is still the same. However, d is no longer the (only) characteristic length, especially for the flow far upstream from the exit. Of course, the width of the fluid is $O(d)$, but another characteristic length, L , emerges, namely the horizontal extent of the fluid outside the channel, which can be much larger than d . In this case, normal stress effects are $O(U\lambda/L) \ll O(U\lambda/d)$, especially for a thin liquid. More precisely, viscoelastic effects should not be important far downstream relatively to channel flow. However, they are expected to be more significant near the channel exit. Thus, and expectedly so, the scale argument indicates that the assumption of Newtonian flow is less valid in the very early transient stages of the free surface flow, but it should hold further downstream.

It is of course desirable to have a numerical implementation that is free of any assumption, where the problem is solved in its entirety as a viscoelastic flow problem. However, the moving boundary problem is extremely difficult to solve in the presence of non-linear effects at high Weissenberg number and inertia, involving a complex constitutive equation such as the JS model. The numerical solution of a highly non-linear involving a moving domain remains challenging despite the efforts in the literature devoted to this important class of problems as encountered in rheology and polymer processing. The simulation of high-Weissenberg flow remains challenging even for problems with fixed domain (with and without a free surface). The BEM loses, in a drastic manner, its advantage over more conventional methods when non-linearity is present. For highly non-linear problems, domain discretization becomes unavoidable, whether the BEM or other methods are used. In this case, remeshing of the domain is required, which adds considerable difficulty to the numerical treatment.

7. CONCLUSION

A hybrid approach consisting of low-order dynamical systems and the BEM is proposed for the simulation of the early stages of blade coating. The stability and bifurcation of PCF of a JS fluid are investigated using the Galerkin projection method. The viscoelastic model used here, displays non-monotonicity of the shear-stress/shear-rate curve, and belongs to the wider class of Oldroyd constitutive models that lead to the destabilization of Couette flow. The viscoelastic velocity profile of the fully developed channel flow is imposed at the exit of the channel as the driving flow for the fluid emerging out of the channel. The fluid is assumed to be Newtonian as it exits the channel. The justification of this assumption is based on the

fact that the magnitude of the rate-of-strain components is relatively small in the free-surface flow region, except perhaps at the exit and at the tip where the free surface meets the moving plate. The BEM is particularly convenient in this case as it allows easy implementation of adaptive meshing or remeshing to determine the evolution of the moving front.

Three characteristic ranges of Weissenberg numbers are identified for the PCF: the pre-critical, the critical and the post-critical ranges. In the pre- and post-critical ranges, the linear Couette flow is unconditionally stable. In these two ranges, the front exhibits a linear shape initially, and eventually swells in the long term. In the critical range, the channel velocity profile is non-linear, leading to strong adverse flow in the coating process near the first critical point. At higher Weissenberg number, the adverse flow weakens, and eventually disappears completely near the second critical point, beyond which linear PCF is restored. The response to suddenly incepted flow shows that the initial transients in the channel flow do not have a significant influence on the coating process.

ACKNOWLEDGEMENTS

This work is supported by the Natural Sciences and Engineering Research Council of Canada.

REFERENCES

1. Kistler SF, Schweizer PM. *Liquid Film Coating*. Chapman & Hall: London, United Kingdom, 1997.
2. Ross AB, Wilson SK, Duffy BR. Blade coating of a power-law fluid. *Physics of Fluids* 1999; **11**:958.
3. Bird RB, Armstrong, RC, Hassager O. *Dynamics of Polymeric Liquids* (2nd edn.), vol. 1. John Wiley & Sons: New York, 1987.
4. Johnson MW, Segalman D. A model for viscoelastic fluid behaviour which allows non-affine deformation. *Journal of Non-Newtonian Fluid Mechanics* 1977; **2**:278.
5. Vinogradov GV, Ya Malkin A, Vanovskii YuG, Borisenkova EK, Yarlykov BV, Berezhneya GV. *Journal of Polymer Science A-2* 1972; **10**:1061.
6. Larson RG. Instabilities in viscoelastic flows. *Rheological Acta* 1992; **31**:213.
7. Kolkka RW, Malkus DS, Hansen MG, Ierley GR. Spurt phenomena of the Johnson-Segalman fluid and related models. *Journal of Non-Newtonian Fluid Mechanics* 1988; **29**:303.
8. Malkus DS, Nohel JA, Plohr BJ. Dynamics of shear flow of a non-Newtonian fluid. *Journal of Computational Physics* 1990; **87**:464.
9. Renardy YY. Spurt and instability in a two-layer Johnson-Segalman liquid. *Theoretical and Computational Fluid Dynamics* 1995; **7**:463.
10. Georgiou GC, Vlassopoulos D. On the stability of the simple shear flow of a Johnson-Segalman fluid. *Journal of Non-Newtonian Fluid Mechanics* 1998; **75**:77.
11. Ashrafi N, Khayat RE. A low-dimensional approach to nonlinear plane-Couette flow of viscoelastic fluids. *Physics of Fluids* 2000; **12**:345.
12. Khayat RE. Finite-amplitude Taylor-vortex flow of viscoelastic fluids. *Journal of Fluid Mechanics* 1999; **400**:33.
13. Floryan JM, Rasmussen H. Numerical methods for viscous flows with moving boundaries. *Applied Mechanics Reviews* 1989; **42**:323.
14. Gabriel M, Dornseifer T, Neunhoffer T. *Numerical Simulation in Fluid Dynamics: A Practical Introduction*. SIAM: Philadelphia, PA, 1997.
15. Khayat RE, Plaskos C, Genouvrier D. An adaptive boundary-element approach to 3D transient free-surface cavity flow, as applied to polymer processing. *International Journal for Numerical Methods in Engineering* 2001; **50**:1347.
16. Khayat RE, Derdouri A. Inflation of hyperelastic cylindrical membranes as applied to blow moulding. Part I. Axisymmetric Case. *International Journal for Numerical Methods in Engineering* 1994; **37**:3773.
17. Power H, Wrobel LC. *Boundary Integral Methods in Fluid Mechanics*. Computational Mechanics Publications: Southampton, 1995.